Journal of
Ceramic Science
and Technology

J. Ceram. Sci. Tech., 04 [04] 197-206 (2013)
DOI: 10.4416/JCST2013-00012
available online at: http://www.ceramic-science.com
© 2013 Göller Verlag

Electrical Resistivity of Si_3N_4-SiC-$MeSi_2$ (Me = Nb, Mo, W, Zr) Composites

E. Zschippang*[1], H. Klemm[1], M. Herrmann[1], S. Höhn[1], B. Matthey[1], U. Guth[2] and A. Michaelis[1]

[1]Fraunhofer Institute for Ceramic Technologies and Systems, Winterbergstraße 28, D-01277, Dresden, Germany
[2]Kurt-Schwabe-Institute for Measuring and Sensor Technology Meinsberg, D- 04720 Ziegra-Knobelsdorf, Germany

received April 15, 2013; received in revised form June 14, 2013; accepted June 28, 2013

Abstract

Si_3N_4-SiC and Si_3N_4-SiC-$MeSi_2$ (Me = Nb, Mo, W, Zr) composites were densified by means of hot pressing at 1840 °C. Additional heat treatment was performed at 1900 °C in a gas pressure furnace at 1900 °C. The hot-pressed and heat-treated composites were investigated with X-ray diffraction, scanning electron microscopy and measurements of their electrical resistivity. The electrical resistivity of the hot-pressed Si_3N_4-SiC composite was about 10^4 Ωcm. The addition of silicides yielded a decrease in composite resistivity to values of about 10^1-10^{-2} Ωcm. The subsequent heat treatment results in a further decrease of the resistivity by at least one order of magnitude for all composites. An $\alpha \rightarrow \beta$ transformation in SiC was detected in the Si_3N_4-SiC-$MeSi_2$ composites with XRD and electron backscatter diffraction (EBSD) analysis. The $\alpha \rightarrow \beta$ transformation in SiC was strongly associated with a high-nitrogen doping concentration of the SiC grains, resulting in lower electrical resistivity of the Si_3N_4-SiC-$MeSi_2$ composites in comparison with the Si_3N_4-SiC composite. Differences in the solution-precipitation process of SiC have been claimed as a reason for the highly doped SiC grains in the Si_3N_4-SiC-$MeSi_2$ composites.

Keywords: Electrical resistivity, silicon nitride, silicon carbide, $a \rightarrow \beta$ transformation, composite

I. Introduction

Si_3N_4 is an excellent material for structural applications. Owing to its high chemical stability as well as high strength and toughness even at high temperatures and good thermal shock resistance, it is particularly suitable for high-temperature applications [1]. Electrically conductive composites for use as ceramic heating elements can be obtained by adding transition metal silicides, such as $MoSi_2$ [2,3]. Si_3N_4-$MoSi_2$ composites have an electrical resistivity of about 10^{-3}-10^{-5} Ωcm and exhibit high oxidation resistance [4]. Unfortunately, the thermal expansion coefficient (CTE) mismatch between Si_3N_4 ($2.5 \cdot 10^{-6}$ K^{-1}) [5] and $MoSi_2$ ($8.25 \cdot 10^{-6}$ K^{-1}) [6] can cause internal stresses in the material during thermal cycling if the component consists of isolating Si_3N_4 and a conducting Si_3N_4- $MoSi_2$ part [7]. Composites made of Si_3N_4 and SiC can be an alternative to the Si_3N_4-$MoSi_2$ composites because the CTE of SiC ($5.3 \cdot 10^{-6}$ K^{-1}) [5] is more similar to that of Si_3N_4. However, the electrical resistivity of Si_3N_4-SiC composites is about 10^7 to 10^3 Ωcm [8,9]. Additionally, special requirements for the electrical properties over a wide temperature range must be met if the composites are to be used as high-temperature heating elements. Si_3N_4-SiC composites usually possess a high negative temperature coefficient of resistivity (NTCR). During heating the electrical resistivity decreases, leading to higher energy release at constant voltage and increasing heating rates. This could ultimately result in burnout of the electrical device [10,11]. Therefore, materials that possess a low NTCR or positive temperature coefficient of resistivity (PTCR) are preferable [10,11]. In general, the electrical resistivity and the temperature dependence of the resistivity of SiC can be decreased by increasing carrier concentration within the crystal lattice [12]. Common dopants used in SiC are aluminium (p-type) and nitrogen (n-type) [13]. Nitrogen concentrations of $4 \cdot 10^{19}$ to $2 \cdot 10^{20}$ cm^{-3} yield electrical resistivity of about 10^{-3} Ωcm in 4H-SiC and 6H-SiC bulk crystals grown with a modified Lely method as reviewed by Rost [14]. In general, in a highly doped n-type semiconductor the Fermi level can be situated in the conduction band and the carriers are fully ionized at all temperatures. The semiconductor is degenerately doped and begins to exhibit metal-like conductivity [12,15,16]. Hence, the temperature coefficient of resistivity increases with temperature owing to scattering effects [12].

In polycrystalline semiconductors, however, the bulk resistance is represented by connection of grain and grain boundary resistances in series [17]. The grain boundaries can significantly affect the resistivity of polycrystalline SiC owing to the formation of potential barriers [18–21]. The

* Corresponding author: eveline.zschippang@ikts.fraunhofer.de

height of the potential barrier is supposed to be determined by the number of dangling bonds or the grain boundary energy and the content of dissolved impurities [22,23]. Accordingly, the resistivity of SiC polycrystalline materials can be reduced by additional annealing reducing the grain boundary defects [17,18,20] and by a high content of nitrogen incorporated in the SiC crystal lattice [20].

For Si_3N_4-SiC composites, a high doping concentration of the SiC grains would also lead to low electrical resistivity and low temperature dependence of resistivity. An electrical resistivity of about 1 Ωcm^{-1} was reported for polysilazane-derived Si_3N_4-SiC composites, most likely as a result of the nitrogen doping of the SiC [24].

Si_3N_4-SiC-$MoSi_2$ composites are considered as an alternative to Si_3N_4-$MoSi_2$ and Si_3N_4-SiC composites [7]. The addition of SiC to a Si_3N_4- $MoSi_2$ matrix reduces internal stresses that occur during thermal cycling caused by the CTE mismatch of Si_3N_4 and $MoSi_2$ [7,25]. Furthermore, the electrical resistivity of the ternary composites is adjustable between several 10^{-3} Ωcm and 10^{12} Ωcm [7]. A great advantage of the Si_3N_4-SiC-$MoSi_2$ composites was the reduced amount of $MoSi_2$ necessary for obtaining low electrical resistivity comparable to that of Si_3N_4-$MoSi_2$ composites [7]. However, up to now the reasons for reduced electrical resistivity of Si_3N_4-SiC-$MoSi_2$ composites have not been adequately investigated.

In this work, Si_3N_4-SiC-$MeSi_2$ (Me = Nb, Mo, W, Zr) composites were made and characterised with regard to their phase composition, microstructure and electrical resistivity. Already small amounts of transition metal silicide result in strong reduction of the electrical resistivity compared to the Si_3N_4-SiC composite. The influence of the transition metal silicides on the solution precipitation process of SiC and hence the doping of the SiC grains was discussed.

II. Experimental

The investigation of the Si_3N_4-SiC composite resistivity was the point of departure for further studies. The composite SC47 containing a SiC volume fraction in excess of the percolation threshold were modified with the addition of 8 vol% $ZrSi_2$ (R=76 · 10^{-6} Ωcm) [26], $MoSi_2$ (R = 22 · 10^{-6} Ωcm) [26], $NbSi_2$ (R = 50 · 10^{-6} Ωcm) [26] or WSi_2 (R = 13 · 10^{-6} Ωcm) [26] in order for ternary composites with lower resistivity to be obtained (Table 1).

Additionally, the influence of the silicide amount on the composite resistivity was investigated based on the substitution of SiC with varying amounts of $MoSi_2$ (2, 4, 8 and 12 vol%).

The Si_3N_4-SiC-$MeSi_2$ composites and SC47 were made from commercial Si_3N_4 (Silzot HQ), SiC (HCST, α-SiC, Grade UF 15), $ZrSi_2$ (HCST), $MoSi_2$ (HCST, Type C), $NbSi_2$ (ABCR, 98 %, 325 mesh), and WSi_2 (ABCR, 99 %). SiO_2 (Heraeus, Pyro Syn) and Yb_2O_3 (Treibach) were added as sintering additives. The starting powders were mixed in isopropanol for 4 h with attrition milling. The slurries were dried and heated up to 800 °C in argon atmosphere to remove the residual organics. All composites were hot-pressed at 25 MPa in a nitrogen atmosphere at temperatures up to 1840 °C. The hot-pressed disc made from the Si_3N_4-SiC-$ZrSi_2$ composite showed a bright rim and a darker centre. Thus specimens were cut from the centres of the hot-pressed discs. One quarter of the hot-pressed discs were heat-treated in a gas pressure furnace at 1900 °C with a nitrogen pressure of 5 MPa for the purposes of generating a coarser microstructure. The relative density was calculated from the ratio of the measured density of the sintered composites with the Archimedes method to their theoretical density. The theoretical density of the composites was estimated from the densities of its components and their weight fractions.

Table 1: Compositions of the composites.

Composite	Conducting phases [vol%]		Non-conducting phases [vol%]	
	SiC	$MeSi_2$	Si_3N_4	SiO_2/Yb_2O_3
SC47	47	0	44	9
$ZrSi_2$-8	39	8	44	9
$NbSi_2$-8	39	8	44	9
WSi_2-8	39	8	44	9
$MoSi_2$-2	45	2	44	9
$MoSi_2$-4	43	4	44	9
$MoSi_2$-8	39	8	44	9
$MoSi_2$-12	35	12	44	9
$MoSi_2$-SN	0	8	83	9

The phase composition of the sintered materials was determined with XRD (XRD 7, Seifert, CuKα; 40 kV, 30 mA, 2θ: 10°– 90°). For this purpose, the samples were crushed and sieved to a fine powder (< 40 μm). Quantitative analysis of the phase composition was conducted with the Rietveld method (Autoquan software, GE Inspection Technologies). The typical relative errors were 7 % for the major components and 10 % – 15 % for the minor components (< 10 vol%); i.e. the silicon carbide and silicon nitride contents were determined with an absolute accuracy of 2 vol%. The accuracy for discrimination between the α-SiC and β-SiC polytype is about 6 % – 10 %.

The cross-sections of the specimens were polished and analysed using an FESEM (NVison 40, Carl Zeiss SMT GmbH). Electron backscatter diffraction (EBSD) was used to distinguish between α-SiC and β-SiC grains in the local microstructures of the subsequently heat-treated Si_3N_4-SiC-$MoSi_2$ composites. The samples were tilted approximately 70° and an acceleration voltage of 10 kV was used. The raw datasets were analysed by means of the software package channel 5 (Oxford Instruments GmbH).

The electrical resistivity was measured with the four-probe method on specimens with dimensions of 4 mm x 4 mm x 20 mm between 20 °C and 800 °C in an Ar atmosphere. A silver braze layer (CB11, Unicore-BrazeTec) was applied as an electrical contact. Two contacts were placed at the 4 mm x 4 mm faces and two small dots on one of the 4 mm x 20 mm faces. Gold wires were then mounted

using an Ag/Pd paste. While the samples were heated in a tube furnace in an argon atmosphere, the electrical resistivity and temperature were measured with a multimeter.

III. Results and Discussion

(1) Sintering

All composites were prepared by means of hot pressing at 1840 °C / 60 min/ 25 MPa in a nitrogen atmosphere. Fig. 1 shows the relative density as a function of time. The analysis of the polished cross-section showed that the porosity was less than 0.5 %.

Si_3N_4-SiC-$MeSi_2$ composites densified faster than the composite SC47. A relative density of about 95 % was achieved for SC47 at 123 min and for $MoSi_2$-8 and $ZrSi_2$-8 at 110 min and 96 min, respectively (Fig. 1).

The faster densification of silicide-modified composites suggests that in addition to an oxide melt, which is responsible for the main densification mechanisms of Si_3N_4 and SiC liquid, Si-containing melt was formed.

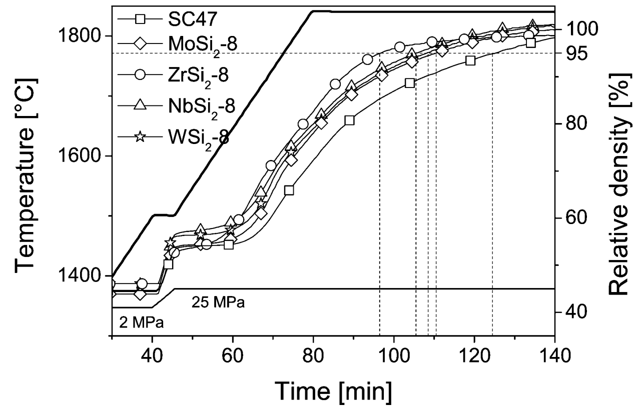

Fig. 1 : The calculated relative density as a function of time.

(2) Phase composition

The XRD results reveal that during sintering the silicides partially decomposed either into the metal nitride, the metal carbide or a metal-rich silicide depending on the nature of the transition metal reacting with residual carbon or nitrogen of the atmosphere. The Rietveld method was used for a quantitative phase analysis. The relative amount of composite's crystalline phases is given in Table 2 and Table 3.

Table 2: Relative amount of crystalline phases in the composites after hot pressing and subsequent heat treatment at 1900 °C (HT). The quantitative phase analysis was determined by means of Rietveld analysis.

Composite	ϱ [Ω cm]	Conducting phases [vol%]					Non-conducting phases [vol%]					
		SiC	$MeSi_2$	Me_5Si_3	MeC	MeN	Si_3N_4	Yb_2SiO_5	$Yb_2Si_2O_7$	$Yb_4Si_2N_2O_7$	$Yb_{4,67}(SiO_4)_3O$	YbSZ
SC47	$3 \cdot 10^4$	49±1					45±1	6±1		13±1		
SC47 HT	$4 \cdot 10^3$	45±1					42±1					
$ZrSi_2$-8	$3 \cdot 10^{-1}$	42±1	5±1			1±1	45±1	4±1	1±1	12±1		2±1
$ZrSi_2$-8 HT	$3 \cdot 10^{-2}$	39±1	4±1			1±1	42±1	1±1				1±1
$NbSi_2$-8	$4 \cdot 10^0$	41±1	6±1		1±1		45±1	7±1		13±1	2±1	
$NbSi_2$-8 HT	$9 \cdot 10^{-2}$	35±2	4±1		1±1		44±2	1±1				
WSi_2-8	$8 \cdot 10^0$	39±2	6±1	1±1	1±1		46±2	7±1		8±1		
WSi_2-8 HT	$6 \cdot 10^{-1}$	39±3	4±1	1±1	1±1		44±1	3±1				

Table 3: Relative amount of crystalline phases in the Si_3N_4-SiC-$MoSi_2$ composites after hot pressing and subsequent heat treatment at 1900 °C (HT) determined by means of Rietveld analysis.

Composite	ϱ [Ω cm]	Conducting phases [vol%]				Non-conducting phases [vol%]					
		SiC	$MoSi_2$	Mo_5Si_3	$Mo_{4.8}Si_3C_{0.6}$	Si_3N_4	SiO_2	Yb_2SiO_5	$Yb_2Si_2O_7$	$Yb_4Si_2N_2O_7$	$Yb_{4,67}(SiO_4)_3O$
$MoSi_2$-2	$1 \cdot 10^3$	46±1	1±1		1±1	45±1		6±1		1±1	
$MoSi_2$-2 HT	$9 \cdot 10^{-2}$	42±2	1±1		1±1	41±1				15±1	
$MoSi_2$-4	$1 \cdot 10^2$	43±1	1±1		2±1	45±1		1±1	5±1	3±1	2±1
$MoSi_2$-4 HT	$2 \cdot 10^{-2}$	41±2	2±1		1±1	45±1				9±1	
$MoSi_2$-8	$1 \cdot 10^1$	39±1	3±1		2±1	47±1		1±1	5±1	3±1	
$MoSi_2$-8 HT	$1 \cdot 10^{-2}$	36±2	3±1		2±1	45±1				14±1	
$MoSi_2$-12	$1 \cdot 10^0$	35±1	7±1		2±1	48±1	3±1		8±1	2±1	2±1
$MoSi_2$-12 HT	$5 \cdot 10^{-3}$	33±1	14±1		1±1	45±1					
$MoSi_2$-SN	$>10^{12}$		5±1	1±1		87±1	5±1	7±1	1±1	11±1	
$MoSi_2$-SN HT	$>10^{12}$		5±1	1±1		77±1					

An overview of the reactions taking place within the composites is given here. A detailed description of the reactions within the Si_3N_4-SiC-$ZrSi_2$ composite has already been published elsewhere [27]. The phase composition of the other composites can be summarized as followed:

Si_3N_4-SiC-$NbSi_2$

During hot pressing, a small amount of $NbSi_2$ reacted with SiC to form NbC. The carbide formation did not noticeably increase during the subsequent heat treatment at 1900 °C.

Si_3N_4-SiC-WSi_2

During sintering, a small amount of WSi_2 decomposed into the metal-rich silicide W_5Si_3 and additionally formed WC. The subsequent heat treatment did not promote further reactions of the remaining WSi_2 to any significant extent.

Si_3N_4-SiC-$MoSi_2$

Besides $MoSi_2$ the metal-rich phase $Mo_{4.8}Si_3C_{0.6}$ was obtained in the Si_3N_4-SiC-$MoSi_2$ hot-pressed and heat-treated composites (Table 3). The subsequent heat treatment in a nitrogen atmosphere caused a considerable transformation from α-SiC (6H) to β-SiC (3C). The SiC reflections often overlapped the reflections of other components, making correct assignment of the SiC polytype more difficult. However, as shown in the X-ray diffraction patterns of $MoSi_2$-12 (Fig. 2), typical reflections of the 6H-SiC phase, the main phase in the starting SiC powder, disappeared and only reflections corresponding to the 3C-SiC (35.6°, 59.9°) were observed for the heat-treated composite. The formation of β-SiC could supported by the Rietveld refinement (Fig. 3) and EBSD-analysis (section 4.3). The $\alpha \rightarrow \beta$ transformation in SiC also agrees with literature data if solution-precipitation of SiC takes place at these temperatures in a nitrogen sintering atmosphere [28, 29]. During heat treatment the formation of a metallic melt was expected from the eutectic temperatures in the system Mo-Si (Table 4). The eutectic temperature of the mixture $MoSi_2$-$Mo_{4.8}Si_3C_{0.6}$-SiC is even lower (1850 °C) [30].

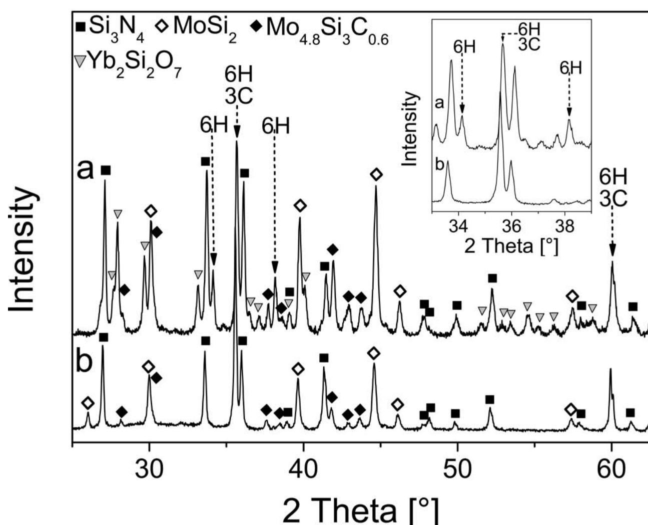

Fig. 2: The x-ray diffraction patterns of $MoSi_2$-12; a) after hot pressing and b) after a subsequent heat treatment at 1900 °C. After the subsequent heat treatment the reflexes of the 6H-SiC-phase disappeared except those that can also associated with the 3C-SiC.

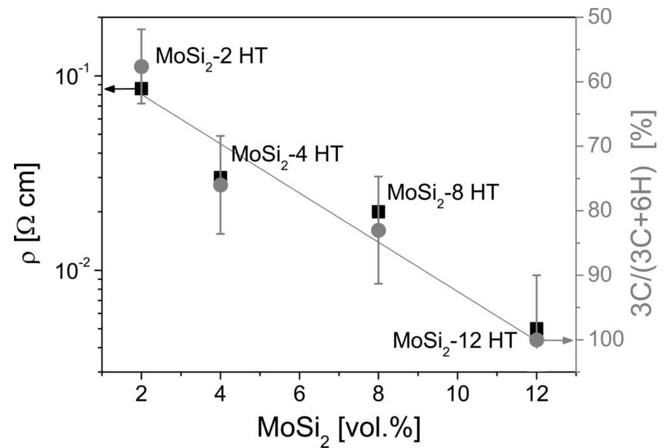

Fig. 3: The electrical resistivity and the proportion of the 3C-SiC indicated as a percentage of the total SiC volume as a function of the added $MoSi_2$ content for the heat treated Si_3N_4-SiC-$MoSi_2$ composites.

Table 4: Melting points and eutectic temperatures of silicides used in this work [46].

	Melting point in °C	Eutectic Phases	Eutectic Temperature [°C]
$ZrSi_2$	1626	$ZrSi_2$ – ZrSi $ZrSi_2$ – Si	1626 1361
$NbSi_2$	1945	$NbSi_2$ – Nb_5Si_3 NbSi2 – Si	1887 1398
$MoSi_2$	2020	$MoSi_2$ – Mo_5Si_3	1900
WSi_2	2160	WSi_2 – W_5Si_3	2010

The amount of β-SiC increased with increasing $MoSi_2$ content and thus with increasing amount of silicide melt during heat treatment (Fig. 3). The used starting SiC powder UF15 contains approximately 70 % of the 6H polytype. A clear distinction of the polytypes in the mixture is difficult. Especially low amounts of 3C are difficult to determine exactly. In the hot-pressed composites the amount of 3C-SiC is low. Only a few 3C-SiC structures were detected with EBSD analysis in some of the Si_3N_4-SiC-$MeSi_2$ composites. But in the case of phase transition during the heat treatment the change could be clearly observed in the XRD pattern.

(3) Microstructure

Fig. 4 shows the SEM images of some of the hot-pressed and heat-treated composites. The grains of the conducting phases SiC, $MoSi_2$, $Mo_{4.8}Si_3C_{0.6}$, $ZrSi_2$ and ZrN appear grey. The $MoSi_2$-, $Mo_{4.8}Si_3C_{0.6}$-, $ZrSi_2$- and ZrN-grains are uniformly grey and slightly larger than the SiC grains. The FESEM in-lens mode reveals a core-rim structure of the SiC grains. The core is brighter than the rim, in contrast to the brighter rim with a higher Al content than that of the darker core described by other authors [31]. This might be connected with the different doping of the SiC (p- versus n-doped semiconductor). The dark regions correspond to the non-conducting Si_3N_4 grains and the oxide grain boundaries.

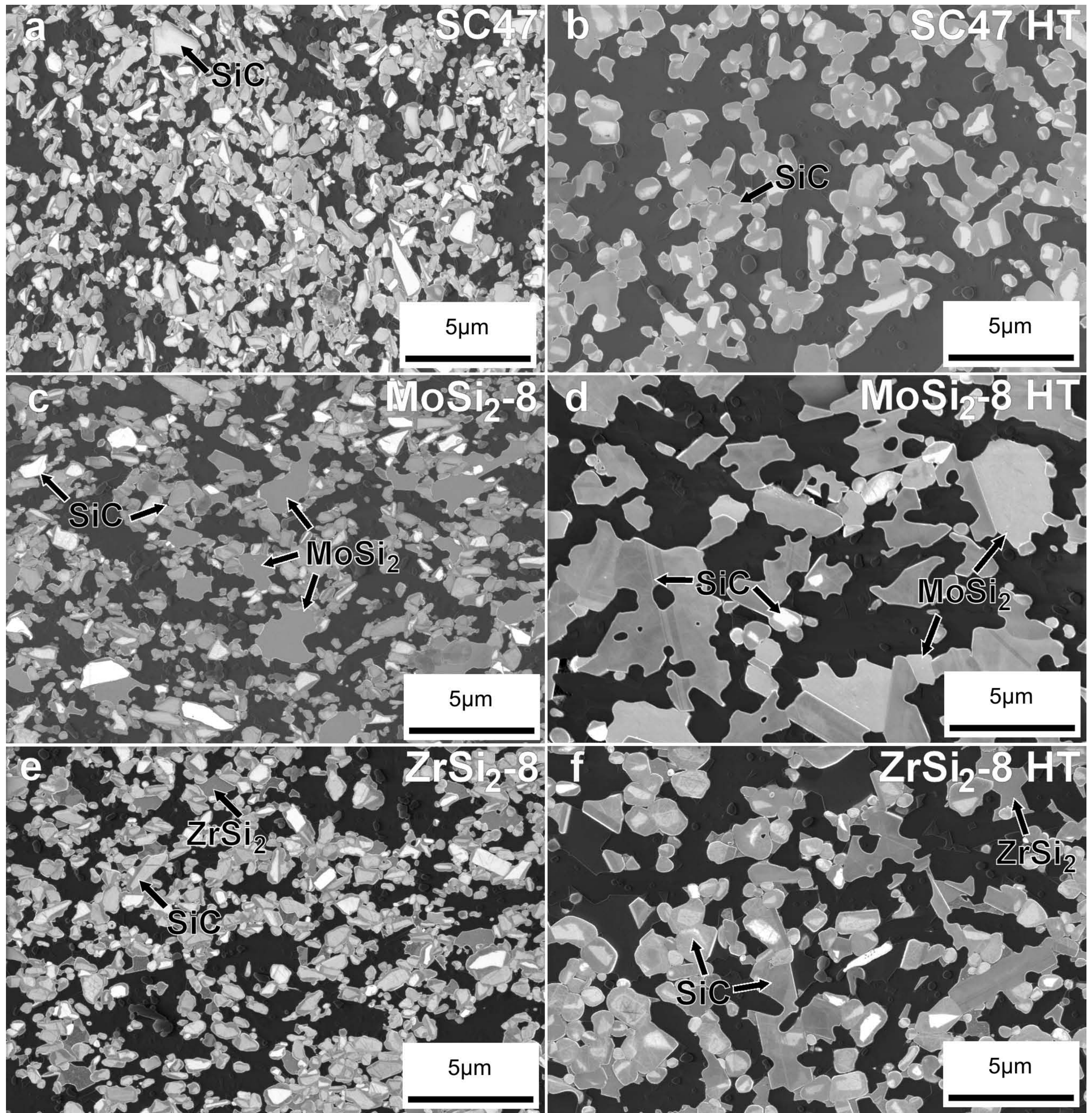

Fig. 4 : The SEM images of the composite after hot pressing a: SC47; c: $MoSi_2$-8; e: $ZrSi_2$-8 and after the subsequent heat treatment at 1900 °C b: SC47-HT; d: $MoSi_2$-8 HT; f: $ZrSi_2$-8 HT. Using an inlens-detector the grains of the conducting phases SiC, $MoSi_2$, $Mo_{4.8}Si_3C_{0.6}$, $ZrSi_2$ and ZrN appear grey. The SiC-grains show a core-rim structure. After the heat treatment, large SiC-structures are formed in composites modified with silicides.

After the subsequent heat treatment the SiC grain size is increased in all composites. The FESEM images show that composites modified with $MoSi_2$ and $ZrSi_2$ consist of some larger SiC structures in addition to the SiC grains with core-rim structure.

The large SiC structures are particularly prevalent in the heat-treated Si_3N_4-SiC-$MoSi_2$ composites and their amount increases with increasing $MoSi_2$ content (Fig. 5). In $MoSi_2$-12 HT nearly all the small SiC grains with core-rim structures disappeared, with only the large SiC structures remaining. Besides, the quantitative phase analysis of $MoSi_2$-12HT revealed a nearly complete transformation of α-SiC to β-SiC (Fig. 3). The $\alpha \rightarrow \beta$ transformation in SiC was confirmed by means of electron backscatter diffraction (Fig. 5). The small SiC grains with core-rim structures were identified as 6H-SiC, whereas the large SiC-structures were identified as β-SiC.

(4) *Electrical resistivity*

Si_3N_4 has a resistivity greater than 10^{12} Ωcm [32]. The addition of 20 vol% SiC resulted in a sharp decrease in electrical resistivity. Further additions of SiC cause only small

changes in resistivity as shown in Fig. 6. Although the electrical resistivity can be obtained in the range of kΩcm, a further decrease in resistivity would be beneficial for applications in many fields. Therefore SC47 is modified with 8 vol% silicides in order to affect the composite resistivity.

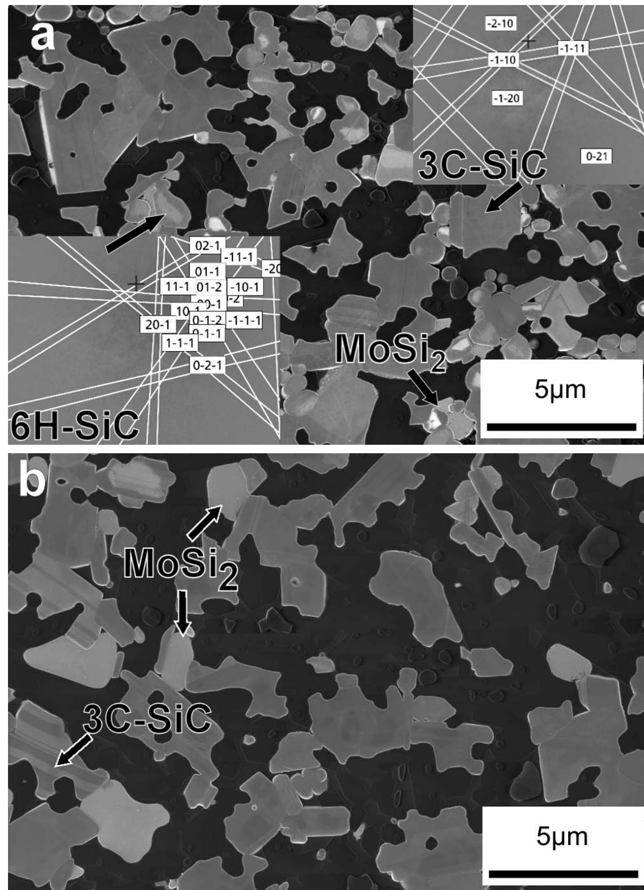

Fig. 5 : The SEM (Inlens) images of the composites after the subsequent heat treatment a) $MoSi_2$-2 HT and b) $MoSi_2$-12 HT. EBSD point measurements were performed at SiC grains with core-rim structure (6H-SiC) and the large irregular formed SiC structures (3C-SiC). A schematic illustration of the Kikuchi bands is shown. In $MoSi_2$-12 HT nearly all 6H-SiC transformed to 3C-SiC.

Fig. 7 shows the electrical resistivity as a function of temperature for SC47 and the silicide-modified composites after hot pressing. SC47 possesses a significant negative temperature coefficient of resistivity (NTCR). At room temperature the resistivity of SC47 is 10^4 Ωcm and at 800 °C 10 Ωcm. The resistivity and the temperature dependence of resistivity was reduced by adding 8 vol% of a metal silicide. The specific resistivity of $MoSi_2$-8, WSi_2-8 and $NbSi_2$-8 is about 10 Ωcm at room temperature and 1 Ωcm at 800 °C. The effect is even more pronounced for $ZrSi_2$-8. $ZrSi_2$-8 has a resistivity of about 10^{-1} Ωcm and the temperature dependence of resistivity is low over the whole temperature range.

As described earlier for a Si_3N_4-SiC-ZrB_2 composite, the electrically conductive pathways are provided predominantly by the three-dimensional SiC network, whereas the grains of the silicide do not form an additional percolating network which might be responsible for a decrease in electrical resistivity [27]. The silicide grains act as additional bridges between the SiC grains, but these bridges do not yield a strong change in the resistivity [27]. The formation of a three-dimensional network of silicide grains in the composites is also excluded, as $MoSi_2$-SN containing 8 vol% $MoSi_2$ but no SiC possesses electrical insulating properties. In comparison, $MoSi_2$-8 containing 8 vol% $MoSi_2$ and 39 vol% SiC offers an electrical resistivity of about 10 Ωcm (Table 3).

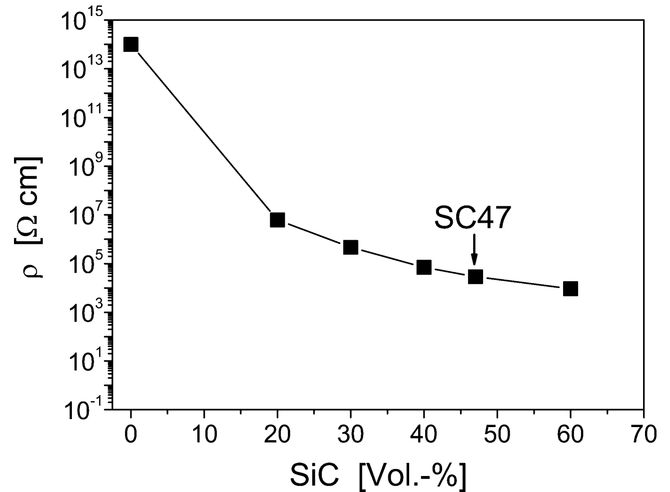

Fig. 6 : The room-temperature resistivity as a function of SiC volume fraction for Si_3N_4-SiC composites. The composite SC47 containing 47 vol% SiC (SC47) was used for further investigations.

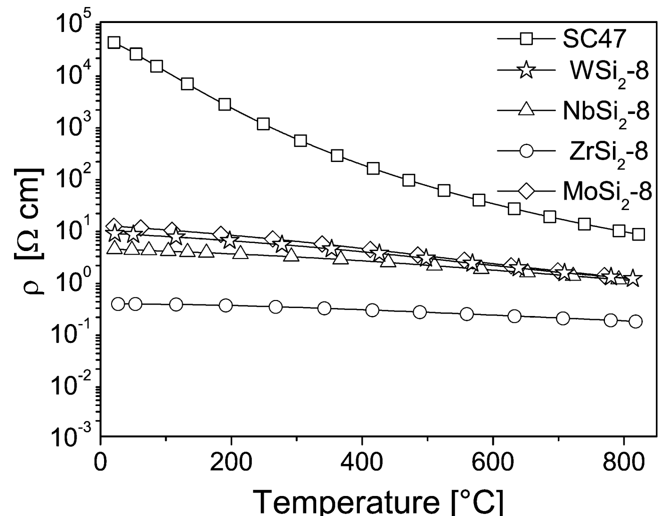

Fig. 7 : The electrical resistivity as function of temperature for the hot-pressed composites.

Accordingly, the conductivity is supposed to depend on the conductivity of the SiC grains itself and the grain boundaries [17]. For thin separating layers (< 10 nm) the resistance of the thin film should be negligible because of tunnelling effects [33, 34]. TEM investigations to determine the thickness of an amorphous grain boundary film were without success. The complicated microstructures consisting of a mixture of many phases make the investigation difficult. Data from literature about the presence of an amorphous grain boundary film in SiC polycrystals are often contradictory [17, 29, 35]. However, the thickness of the amorphous grain boundary film measured with TEM was reported in the range of less than 3 nm [36, 37], i.e. much lower than the critical value. In the case of grain boundaries consisting of the same material as the grains but containing

defects and dopants, the grain boundary resistivity strongly depends on the doping concentration of the adjacent SiC grains [20, 22]. Hence the impact of the grain boundaries on the composite resistivity is very difficult to estimate.

On the other hand, low resistivity and low temperature dependence of the resistivity imply that the SiC grains are highly conductive owing to a high carrier concentration [14]. The doping of the SiC grains depends on the activity of the doping element around the SiC grains and on the kinetics of the doping process.

The diffusion of the doping elements into SiC grains is slow [38], i.e. less than 10^{-16} cm² s^{-1} below 2000 °C [39]. Hence, the doping is supposed to occur during the solution-precipitation process. This process takes place via the oxynitride or a metal liquid.

In the silicide-free composite SC47 the solution-precipitation took place via an oxynitride liquid, resulting in a specific resistivity of $4 \cdot 10^4$ Ωcm after hot pressing and $5 \cdot 10^3$ Ωcm after the heat treatment (Fig. 7, Fig. 8). No large 3C-SiC structures were observed even after the heat treatment (Fig. 4). These observations prove a slow solution precipitation process of SiC grains. The Si_3N_4-SiC-$MeSi_2$ composites were sintered at a temperature near the melting point of the transition metal silicides (Table 4). During sintering, a Si-containing melt enhances the solution precipitation of Si_3N_4 and SiC and thus the densification of the composites (Fig. 1).

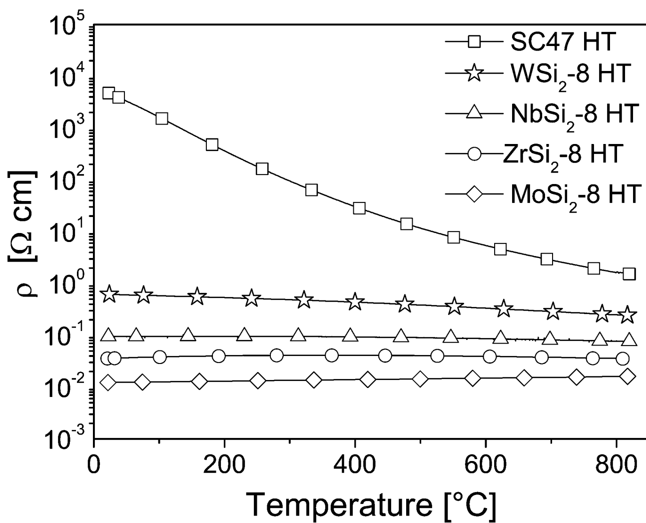

Fig. 8 : The electrical resistivity as function of temperature for the heat treated (HT) composites.

The measured phase compositions reveal that the Si-containing melt during sintering will not have the chemical composition of the added transition metal silicide. For Mo and W, a second silicide was observed, indicating that the Me/Si ratio was somewhere between 1:2 and 1:0.6. In the case of the zirconium silicide a small amount of Si was also observed, as described elsewhere [27]. Therefore in all systems, formation of a silicide melt is reasonable. It is known that up to 0.01 wt% nitrogen can be dissolved in liquid silicon at 1542 °C [40, 41]. Therefore the nitrogen doping is supposed to be achieved via the presence of a nitrogen-containing metallic melt from which the doped SiC recrystallized [28].

It is assumed that the doping process was kinetically controlled. Evidence for that was that the addition of transition metal silicides results in enhanced densification and in a decrease in resistivity (Fig. 1, Fig. 7). This was most pronounced for $ZrSi_2$-8, containing the silicide with the lowest melting point (Table 4). In this system the formation of a high amount of silicide melt even during hot pressing is reasonable whereas in the other composites a smaller or even no amount of silicide liquid could be expected during hot pressing (Table 4).

Furthermore the composite resistivity depends on the amount of silicides added. As shown for Si_3N_4-SiC-$MoSi_2$ composites with 2, 4, 8 and 12 vol% $MoSi_2$ the resistivity decreases with an increasing amount of silicide (Fig. 9).

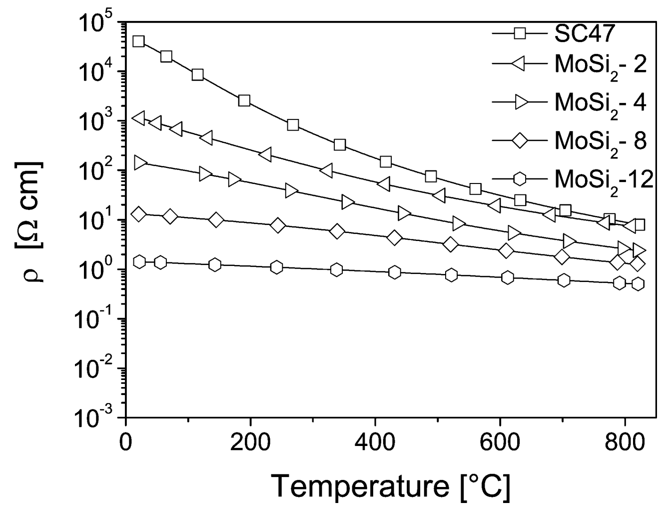

Fig. 9 : The electrical resistivity as function of temperature for the hot-pressed Si_3N_4-SiC-$MoSi_2$ composites.

Another sign for a kinetically controlled doping process was that the electrical resistivity of the composites decreases owing to the subsequent heat treatment at 1900 °C (Fig. 8). Especially the heat-treated Si_3N_4-SiC-$MoSi_2$ composites have a resistivity of less than about 10^{-1} Ωcm with only a weak temperature dependence between 25 °C and 800 °C (Fig. 10). $MoSi_2$-8 HT and $MoSi_2$-12 HT have a positive temperature coefficient of resistivity (PTCR) and the resistivity increases with increasing temperature.

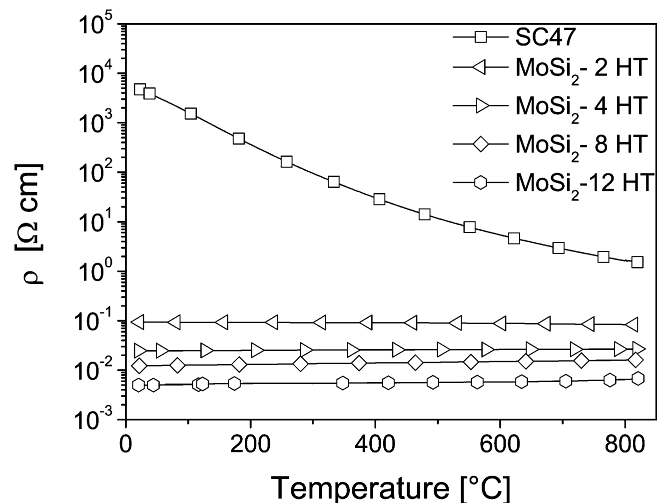

Fig. 10 : The electrical resistivity as function of temperature for the heat treated (HT) Si_3N_4-SiC-$MoSi_2$ composites.

Also the difference in resistivity between $ZrSi_2$-8 and some other Si_3N_4-SiC-$MeSi_2$ composites become smaller owing to the heat treatment at 1900 °C at which the other transition metal silicides were also liquid (Fig. 8). The highest resistivity of the silicide-containing materials after heat treatment has the WSi_2-8 HT material, which contains the most refractive silicide (Table 4).

The presence of liquid phases over a longer period during the heat treatment could promote the solution-precipitation process and the doping of SiC grains as well as the annealing of lattice defects and dangling bonds at the SiC grain boundaries [17]. It is proposed that this causes the low resistivity of $ZrSi_2$-8 and it is suggested as an explanation for the decrease in the composite resistivity owing to a subsequent heat treatment at 1900 °C in general. However, with increasing $MoSi_2$-content the electrical resistivity still decreases. Also the 3C-SiC content in the composites increases with increasing $MoSi_2$ volume fraction. The greatest amount of 3C-SiC, i.e. the strongest solution precipitation process of SiC was observed for $MoSi_2$-12 HT resulting in the lowest resistivity (Fig. 3).

These data suggest that the doping process was not finished for the compositions with lower $MoSi_2$ amounts, and was kinetically controlled even during heat treatment at 1900 °C.

Besides the kinetics, the nitrogen activity within the composite determines the doping level and hence the conductivity of the SiC grains.

During sintering an equilibrium is established between Si_3N_4, the nitrogen gas pressure $p(N_2)$ in the sintering atmosphere and the silicon and nitrogen activity in the Si-containing metallic melt [40,41].

Assuming that the nitrogen dissolved in the Si-containing melt is in equilibrium with the nitrogen in the sintering atmosphere:

$$\mu(N_2(\text{dissolved})) = \mu(N_2(g)) \quad (1)$$

This results in the equation between nitrogen activity (a) and nitrogen gas pressure [42]

$$a(N_2(\text{dissolved})) \sim p(N_2) \quad (1a)$$

The equilibrium nitrogen pressure can be calculated based on the observed phases. The existence of the two silicides and silicon nitride equivocally determine the nitrogen pressure at a given temperature based on the equations:

$$15MeSi_2 + 14N_2 \rightleftarrows 3Me_5Si_4 + 7Si_3N_4 \quad (2)$$

Me = Mo, W, Nb

$$3ZrSi_2 + 2N_2 \rightleftarrows 3ZrSi + Si_3N_4 \quad (3)$$

The calculated partial pressures are given in Fig. 11. Of course, for the molten state this is only an approximation, but no strong derivations would be expected.

The calculated equilibrium partial pressure and therewith the nitrogen activity is about one magnitude higher for the Si_3N_4-SiC-$MoSi_2$ composites than for the other materials. Since the doping depends on the activity of the dopants, the higher nitrogen activity is assumed to significantly affect the doping and hence the conductivity of the SiC grains. This explains why the resistivity of the Si_3N_4-SiC-$MoSi_2$ composites was particularly low.

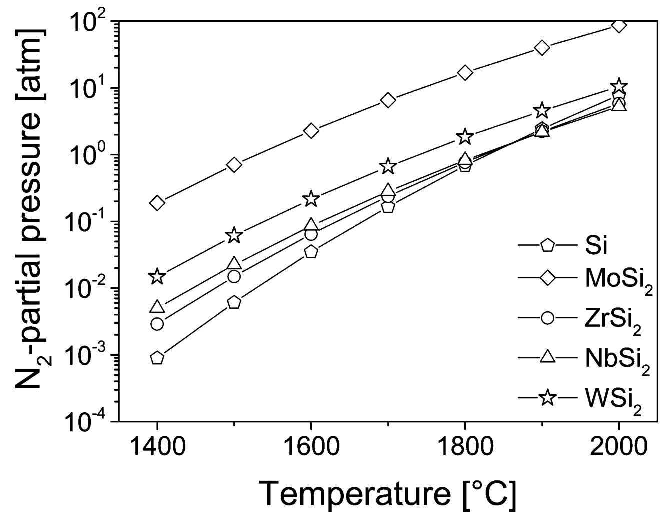

Fig. 11: The calculated equilibrium partial pressures (FactSage 6.3 equilib module) for the solid phases $MeSi_2/Me_5Si_3/Si_3N_4$ (Me = Mo, W, Nb) and $ZrSi_2/ZrSi/Si_3N_4$ and Si/Si_3N_4 between 1400 °C and 2000 °C are depicted as a line+symbol graph. The nitridation of silicon (Si) and the silicides ($MeSi_2$) starts, when the nitrogen partial pressure exceeds the lines.

It was not possible to determine the nitrogen doping concentration in the SiC up to now. However, the $\alpha \rightarrow \beta$ transformation in SiC that was most pronounced for the Si_3N_4-SiC-$MoSi_2$ composites hints at the high nitrogen doping concentration. The $\alpha \rightarrow \beta$ transformation in highly nitrogen-doped alpha SiC was already reported by several groups [16, 43, 44]. Alexander [16,44] ascertained that in 6H-SiC, it was not possible to achieve a nitrogen concentration greater than $6 \cdot 10^{19}$ cm^{-3} was because nitrogen pressures adequate to give doping in this range would lead to the formation of the β-SiC polytype. The relationship between nitrogen doping and the stability of the β-SiC is also shown by Kim [34]. The carrier concentration and the resistivity of the nitrogen-doped β-SiC were about 10^{20} cm^{-3} and 10^{-3} Ωcm, respectively [45].

In this work, an $\alpha \rightarrow \beta$ transformation in SiC was particularly observed in Si_3N_4-SiC-$MeSi_2$ composites after a subsequent heat treatment was applied. The composites have a resistivity of less than about 10 Ωcm and the temperature dependence of resistivity is low (Fig. 8). All this is evidence that the conductivity of the SiC network in the material is increased owing to a higher doping level of the SiC formed by the solution precipitation.

IV. Conclusions

Si_3N_4-SiC composites having a resistivity of about 10^4 Ωcm were modified with the addition of 8 vol% silicides. The addition of silicides results in a decrease in resistivity to about $10^1 - 10^{-2}$ Ωcm. The composite resistivity was further decreased to a value of about 10^{-2} Ωcm when subsequent heat treatment at 1900 °C in a nitrogen atmosphere was applied. The resistivities of the silicide-modified composites are less temperature-dependent than that of the Si_3N_4-SiC composites.

The silicide addition significantly affected the phase composition and microstructure of the composite as shown by XRD and FESEM analyses. An $\alpha \rightarrow \beta$ transformation in SiC was detected in the subsequently heat-treated composites by means of electron backscatter diffraction

(EBSD). The amount of β-SiC increases with an increasing $MoSi_2$ volume and is associated with a decrease in resistivity. Therefore it is assumed that the α → β transformation indicate a high nitrogen doping concentration in the SiC grains.

References

1 Klemm, H.: Silicon nitride for high-temperature applications, *J. Am. Ceram. Soc.*, **93**, 1501 – 1522, (2010).

2 Manukyan, K.V., Kharatyan, S.L., Blugan, G., Kocher, P., Kuebler, J.: $MoSi_2$-Si_3N_4 Composites: influence of starting materials and fabrication route on electrical and mechanical properties, *J. Eur. Ceram. Soc.*, **29**, 2053 – 2060, (2009).

3 Kao, M.Y.: Properties of silicon nitride-molybdenum disilicide particulate ceramic composites. *J. Am. Ceram. Soc.*, **76**, 2879 – 2883, (1993).

4 Guo, Z.Q., Blugan, G., Grauble, T., Reece, M., Kuebler, J.: The effect of different sintering additives on the electrical and oxidation properties of Si_3N_4-$MoSi_2$ composites. *J. Eur. Ceram. Soc.*, **27**, 2153 – 2161, (2007).

5 Holleck, H.: Material selection for hard coatings, *J. Vac. Sci. Technol.*, **A4**, 2661 – 2669, (1986).

6 Neshpor, V.S., Reznichenko, M.I.: Investigating the thermal expansion of some silicides, *Refractories*, **4**, 145 – 148, (1963).

7 Klemm, H., Bales, A., Martin, H.P., Herrmann, M.: Electrically conductive ceramic composite (in German). DE 102006062371A1, (2006).

8 Sawaguchi, A., Toda, K.: Mechanical and electrical-properties of silicon-nitride silicon-carbide nanocomposite material, *J. Am. Ceram. Soc.*, **74**,1142 – 1144, (1991).

9 Yamada, K., Kamiya, N.: High temperature mechanical properties of Si_3N_4-$MoSi_2$ and Si_3N_4-SiC composites with network structures of second phases, *Mat. Sci. Eng. A-Struct.*, **261**, 270 – 277, (1999).

10 Heuberger, M., Kuntz, M., Nass, R.: Silicon carbide element (in German), DE 19956767A1, (2001).

11 Willkens, C.A., Bateman, L.S.: Composition for small ceramic ignitors. US 005514630A, (1996).

12 Shor, J.S., Goldstein, D., Kurtz, A.D.: Characterization of n-type beta-SiC as a piezoresistor, *IEEE T. Electron Dev.*, **40**, 1093 – 1099 (1993).

13 Casady, J.B., Johnson, R.W.: Status of silicon carbide (SiC) as a wide-bandgap semiconductor for high temperature applications: A review, *Solid-State Electronics*, **39**, 1409 – 1422, (1996).

14 Rost, H.J., Schulz, D., Siche, D.: High Nitrogen Doping During Bulk Growth of SiC. In: Silicon Carbide – Recent Major Advances. Springer-Verlag, Berlin Heidelberg New York, Germany, 2004.

15 Da Silva, A.F., Pernot, J., Contreras, S., Sernelius, B.E., Persson, C., Camassel, J.: Electrical resistivity and metal-nonmetal transition in n-type doped 4H-SiC, *Phys. Rev. B*, **74**, 245201, (2006).

16 Alexander, M.N., Holcomb, D.F.: Semiconductor-to-metal transition in n-type group IV semiconductors, *Rev. Mod. Phys.*, **40**, 815 – 829, (1968).

17 Siegelin, F., Kleebe, H.J., Sigl, L.S.: Interface characteristics affecting electrical properties of Y-doped SiC, *J. Mater. Res.*, **18**, 2608 – 2617, (2003).

18 Kleebe, H.J., Siegelin, F.: Schottky barrier formation in liquid-phase-sintered silicon carbide, *Z. Metallkd.*, **94**, 211 – 217, (2003).

19 Kobayashi, R., Tatami, J., Wakihara, T., Komeya, K., Meguro, T., Tu, R., Goto, T.: Evaluation of grain-boundary conduction of dense AlN-SiC solid solution by scanning nonlinear dielectric microscopy, *J. Am. Ceram. Soc.*, **93**, 4026 – 4029, (2010).

20 Kondo, A.: Electrical conduction mechanism in recrystallized SiC, *J. Ceram. Soc. Jpn.*, **100**, 1225 – 1229, (1992).

21 Schroeder, A., Pelster, R., Grunow, V., Lennartz, W., Nimtz. G., Friederich. K.: Charge transport in silicon carbide: atomic and microscopic effects, *J. Appl. Phys.*, **80**, 2260 – 2268, (1996).

22 Clarke, D.R.: Varistor ceramics, *J. Am. Ceram. Soc.*, **82**, 485 – 502, (1999).

23 Pike, G.E.: Semiconducting polycrystalline ceramics. In: Materials Science and Technology. Wiley-VCH Verlag, 1994.

24 Haluschka, C., Engel, C, Riedel, R.: Silicon carbonitride ceramics derived from polysilazanes Part II. Investigation of electrical properties, *J. Eur. Ceram. Soc.*, **20**, 1365 – 1374, (2000).

25 Hebsur, M.G.: Development and characterization of SiC(f)/$MoSi_2$-Si_3N_4(p) hybrid composites, *Mater. Sci. Eng.*, **A**, **261**, 24 – 37, (1999)

26 Samsonov, G.V: Handbook of refractory compounds. IFI/ Plenum, New York, 1980.

27 Zschippang, E., Klemm, H., Herrmann, M., Sempf, K., Guth, U., Michaelis, A.: Electrical resistivity of silicon nitride – silicon carbide based ternary composites, *J. Eur. Ceram. Soc.*, **32**, 157 – 165, (2012).

28 Jeon, Y.S., Shin, H., Lee, Y.H., Kang, S.W.: Reduced electrical resistivity of reaction-sintered SiC by nitrogen doping, *J. Mater. Res.*, **23**, 1020 – 1025, (2008).

29 Jepps, N.W., Page, T.F.: The 6H-3C "Reverse" transformation in silicon carbide compacts, *J. Am. Ceram. Soc.*, **64**, C177 – C178, (1981).

30 Gnesin, G.G.: Karbidokremnievye materialy. Metallurgija, Moscow, 1977.

31 Ihle, J., Martin, H.P., Herrmann, M., Obenaus, P., Adler, J., Hermel, W., Michaelis, A.: The influence of porosity on the electrical properties of liquid-phase sintered silicon carbide, *Int. J. Mater. Res.*, **97**, 649 – 656, (2006).

32 Thorp, J.S., Sharif, R.I.: D.C. electrical properties of hot-pressed nitrogen ceramics, *J. Mater. Sci.*, **13**, 441 – 449, (1978).

33 Can, A.: Densification, microstructure and properties of liquid-phase sintered silicon carbide materials [PhD-Thesis]. University of Witwatersrand, Johannesburg, 2004.

34 Dietrich, I.: Measurement of the resistance of thin insulating layers between gold contacts in the range of the tunnel effect, (in German), *Zeitschrift für Phys. A Hadron Nucl.*, **132**, 231 – 238, (1952).

35 Kleebe, H.J.: Comparison between SEM and TEM imaging techniques to determine grain-boundary wetting in ceramic polycrystals, *J. Am. Ceram. Soc.*, **85**, 43 – 48, (2002).

36 Moberlychan, W.J., De Jonghe, L.C.: Controlling interface chemistry and structure to process and toughen silicon carbide, *Acta Mater.*, **46**, 2471 – 2477, (1998).

37 Pezzotti, G., Kleebe, H.-J., Ota, K.: Grain boundary viscosity of polycrystalline silicon carbides, *J. Am. Ceram. Soc.*, **81**, 3293 – 3299, (1998).

38 Tian, Z., Quick, N.R., Kar, A.: Laser-enhanced diffusion of nitrogen and aluminum dopants in silicon carbide, *Acta Mater.*, **54**, 4273 – 4283, (2006).

39 Kroko, L.J., Milnes, A.G.: Diffusion of nitrogen into silicon carbide single crystals doped with aluminium, *Solid-State Electronics*, **9**, 1125 – 1134, (1966).

40 Dalaker, H., Tangstad, M.: Temperature dependence of the solubility of nitrogen in liquid silicon equilibrated with silicon nitride, *Mater. T. JIM*, **50**, 2541 – 2544, (2009).

[41] Narushima, T., Ueda, N., Takeuchi, M., Ishii, F., Iguchi, Y.: Nitrogen solubility in liquid silicon, *Mater. T. JIM,* **35**, 821 – 826, (1994).

[42] Herrmann, M., Goeb, O.: Colour of gas-pressure-sintered silicon nitride ceramics, part II. thermodynamic considerations, *J. Eur. Ceram. Soc.,* **21**, 461 – 469, (2001).

[43] Kuhr, T.A., Liu, J., Chung, H.J., Skowronski, M., Szmulowicz, F.: Spontaneous formation of stacking faults in highly doped 4H-SiC during annealing, *J. Appl. Phys.,* **92**, 5863 – 5871, (2002).

[44] Alexander, M.N.: Nuclear-Magnetic-Resonance study of heavily nitrogen-doped silicon carbide, *Phys. Rev.,* **172**, 331 – 340, (1968).

[45] Kim, K.J., Lim, K.Y., Kim, Y.W.: Effective nitrogen doping for fabricating highly conductive b-SiC ceramics, *J. Am. Ceram. Soc.,* **94**, 3216 – 3219, (2011).

[46] Villars, P., Okamoto, H., Cenzual, K.: A-B-C phase diagram, ASM Alloy Phase Diagrams Center, ASM International, Materials Park. *http://www1.asminternational.org/AsmEnterprise/APD* 2006.